

Solid-state single photon sources: light collection strategies

W.L. Barnes^{1,a}, G. Björk², J.M. Gérard³, P. Jonsson², J.A.E. Wasey¹, P.T. Worthing¹, and V. Zwiller⁴

¹ Thin Film Photonics Group, School of Physics, University of Exeter, Exeter, EX4 4QL, UK

² Dept. of Microelectronics and Information Technology, KTH Electrum 229, 16440 Kista, Sweden

³ CNRS/LPN, 196 avenue Henri Ravera, B.P. 29, 92222 Bagneux Cedex, France

⁴ Dept. of Solid State Physics, Lund University, 22100 Lund, Sweden

Received 19 July 2001 and Received in final form 5 October 2001

Abstract. We examine the problem of efficiently collecting the photons produced by solid-state single photon sources. The extent of the problem is first established with the aid of simple physical concepts. Several approaches to improving the collection efficiency are then examined and are broadly categorized into two types. First are those based on cavity quantum dynamics, in which the pathways by which the source may emit a photon are restricted, thus channeling emission into one desired mode. Second are those where we try to reshape the free space modes into a target mode in an optimal way, by means of refraction, without fundamentally altering the way in which the source emits. Respectively, we examine a variety of microcavities and solid immersion lenses. Whilst we find that the micropillar microcavities offer the highest collection efficiency ($\sim 70\%$), choosing this approach may not always be appropriate due to other constraints. Details of the different approaches, their merits and drawbacks are discussed in detail.

PACS. 03.67.Dd Quantum cryptography – 42.79.Gn Optical waveguides and couplers – 12.20.-m Quantum electrodynamics

1 Introduction

The emission of light is central to a wide range of technologies and continues to provide a fascinating and important area of research. A particularly topical aspect is spectroscopy at the single molecule level and is of interest in chemistry and biology as well as physics [1]. This level of control over optical sources has led to the prospect of new applications, notably the single photon source. Such sources would be valuable in many areas, *e.g.* as standards for light detection, for sub-shot noise measurements, for testing quantum mechanics and in the field of quantum information. In the latter area the source is a vital component in the development of quantum cryptography, more accurately referred to as quantum key distribution (QKD). This is perhaps the first application of truly quantum concepts to provide the potential for an entirely new way of communicating. The basic idea is to transfer information at the level of single quanta, making direct use of quantum mechanics to prevent the secret key being broken. Most implementations rely on photons as the quanta, as is clear from the many articles in this special issue. There are two ways in which we may attempt to produce a train of single photons, attenuated lasers and sources based on single emitters.

1.1 Attenuated lasers sources

Here a pulsed laser beam is simply attenuated with neutral density filters until there is on average a fraction of a photon per pulse [2]. This technique requires no new technology, provides a well-directed output, is narrow band and can be accomplished at almost any desired wavelength. Despite these numerous attributes, attenuated laser beams suffer from one important drawback; that of exhibiting Poissonian statistics. Not all the attenuated pulses contain one photon, many will contain zero photons thus limiting the effective data rate for key distribution. More seriously, some pulses will contain two or more photons. The problem here is that multiple photon pulses offer the prospect of undetected eavesdropping. Increasing the attenuation to further limit the number of multiple photon pulses helps, but does not altogether remove the problem, since this yields even more “empty” pulses.

1.2 Sources based on single emitters

To overcome the multiple photons per pulse problem one has to switch to sources that are only capable of emitting one photon at a time. Spontaneous emission from a single molecule is a simple example; the molecule is first excited, it then decays to produce a photon, after which it can be re-excited to produce the next photon etc. Emission based on a single molecule does not follow Poissonian

^a e-mail: w.l.barnes@ex.ac.uk
or e-mail: w.l.barnes@exeter.ac.uk

statistics since there is zero probability for the production of multiple photons. Such sources are said to exhibit “anti-bunching”, since the photons cannot be bunched together more than one at a time [3]. Whilst the attractions of such a source for quantum key distribution are clear, their implementation is not without difficulties. Particularly important for us is the fact that whilst an attenuated laser beam is directional and therefore easily collected, emission from single emitters is often well approximated as omni-directional; this is at the heart of the problem of collection efficiency. As might be imagined, research in this area has overlap with that in others, notably single molecule spectroscopy.

Single molecules are not the only emitter sources; other elegant solutions have been both proposed and developed, notably emitters that make use of our impressive ability to manipulate electronic states in semiconductors through nanoscale control of materials and device geometry. The basic idea is to limit the number of charge carriers entering a device so that only one exciton can be formed at a time. If this can be accomplished only one photon is produced when the exciton decays *via* radiative recombination. Use of the Coulomb blockade has been proposed [4] and demonstrated [5] to inject single charge carriers whilst others have made use of the Pauli exclusion principle [6]. Although the feature of only one exciton at a time may be thought to be an essential requirement for single photon emission, this is not so. Quantum dots may also be used in which rather than limiting the number of charge carriers in the device at any one time spectral strategies are deployed to ensure only emission from one exciton is used. This can be achieved because interactions between excitons lead to different exciton energies, the last exciton to decay having a unique emission frequency that can be selected with appropriate spectral filtering [7,8].

1.3 The requirements of a single photon source

To produce single photons on demand we need to accomplish several things; we have to,

- (a) isolate a single emitter;
- (b) excite the single emitter;
- (c) collect and direct the emitted photons into the optical system to be used for key distribution.

We might also consider other desirable attributes such as a narrow emission wavelength to allow filtering to be used at the detection end of the quantum channel; this helps to reduce background noise levels. Some schemes also require the photons to be in a well-defined polarization state; a high quantum efficiency emitter would also be desirable. In addition, knowing when to expect the photon would be very useful to allow time-gated detection. This last aspect requires either a very short fluorescence lifetime or the use of parametric down conversion; one photon is used to encode information the other to act as a timing trigger [9]. Whilst these are all fascinating topics in their own right, for the purpose of the present article we will focus on the collection efficiency.

1.4 State of the art

To date several groups have demonstrated generation of single photons using a variety of emitters. There are schemes based on single molecules [10,11], or single defect sites [12,13], those based on quantum dots (artificial atoms) [7,8,14,15] (see also the article by Gérard *et al.* in this issue) quantum wells [5] and nano-crystals [16]. It is not our purpose to review all of these reports here; rather we simply note some of the important characteristics these sources exhibit. First and foremost, the schemes demonstrated thus far have in general rather low collection efficiencies, typically of order 1%. To remedy this low efficiency it is important to understand the nature of the problem, a problem that can be viewed in two ways.

The coupling between atoms, molecules etc. and optical radiation is in general rather poor simply because of the significant size mismatch between atomic wavefunctions and the wavelength of the emitted radiation. This is a fundamental fact that cannot be “engineered away”. Rather we have to devise strategies to cope with it. Synthetic atoms such as quantum dots have larger sizes, but there is still a big mismatch. The problem caused by this mismatch is that in general we wish to generate not just any photon; we want to generate a single optical mode, typically that of an optical fiber. Our task is then to distort the modes into which emission may take place by adjusting the local photonic environment. We can see how such a distortion may be effective by recalling Fermi’s Golden rule,

$$\Gamma_{ij} \propto |M_{ij}|^2 \rho(\omega_{ij}) \quad (1)$$

Γ_{ij} is the rate of spontaneous emission (*i.e.* the probability of emission), M_{ij} is the matrix element that connects the excited and ground states of the emissive species *via* the radiative decay channel (usually an electric dipole transition) and $\rho(\omega_{ij})$ is the photonic mode density at the emission frequency ω_{ij} . For the case of emission in free space, all directions of emission are allowed and there will be a poor match to the single mode of our desired optical system. Viewing the problem in this way leads one to think of physical solutions, *i.e.* ways in which the physical (photonic) environment may be manipulated to adjust the modes into which spontaneous emission may take place. Such manipulation is at the heart of cavity Quantum Electrodynamics (cavity QED). Consequently, we often refer to physical solutions to the collection problem as CAVITY QED approaches.

It is our purpose to review the ways in which this may be done. Before doing so it is worth looking at this problem from an alternative perspective. In its simplest sense our single emitter amounts to a very well localized source that emits photons isotropically. There are good practical reasons why it is convenient to confine our emitter to a solid medium; principally this helps us locate and isolate the source. We are thus faced with an immediate problem; how to get the light out of this material and into our (single mode) optical system. To see the nature of the problem we refer to Figure 1. Photons emerging such as

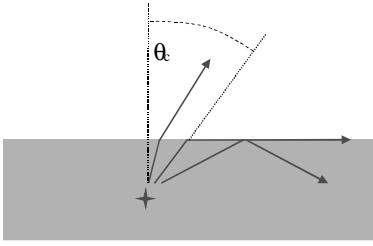


Fig. 1. The total internal reflection problem for light emerging from within a slab of material. Emission directions are restricted to those below the critical angle θ_c .

to make an angle of more than the critical angle with the normal will be totally internally reflected. A simple analysis of this problem leads to an estimate of the fraction of emission that escapes the material surface as $1/2n^2$, n being the refractive index of the material, emission being assumed to take place into air. For an organic material this may amount to 20% whilst for an inorganic semiconductor such as GaAs it may be no more than 3%; it can thus be an acute problem. Indeed, the situation is likely to be worse than this since not all light emerging from the material is likely to fit the numerical aperture of the collection system. It is principally for this reason that most reported collection efficiencies have been estimated at $<1\%$. Viewing the collection problem in this geometric way naturally leads one to think of geometric solutions. These exist, particularly in the form of the solid immersion lens, and will be discussed in Section 3.

Having established the nature of the problem we may now look at how it may be overcome; there is a large literature on this topic in the context of improving the efficiency of other optical sources, notably the light emitting diodes [17]. Not all of the approaches used to improve emission from LEDs may be used in the context of single photon sources owing to the spatial resolution required for the collection optics in order to isolate a single source; this will be discussed further in Section 2.2. We begin Section 2 by looking at physical or Cavity QED approaches to the collection problem; geometrical approaches will be discussed in Section 3.

2 Improving the collection efficiency – cavity QED approaches

Altering the local electromagnetic boundary conditions changes the photonic mode density in the neighbourhood of an emitter, something we hope to do to our advantage. The logical extreme of such an approach is a useful conceptual starting point, something we may call the “ideal photonic box” with which we could ensure the perfect collection of the emission from a radiating dipole. The box provides three-dimensional confinement of electromagnetic radiation and leads to the formation of a discrete series of confined modes. If these modes are well separated spectrally on the scale of the emitter linewidth, and if the emitter is coupled to a non-degenerate confined

mode then only a single pathway will exist for the radiative de-excitation of this emitter: all photons will be emitted into this single cavity mode.

As proposed by Yablonovitch [18], this ideal situation could be achieved by using a 3D photonic crystal as a perfect mirror, and a tailored defect within this crystal to define the cavity. Besides being collected in an ideally efficient way, emitted photons would also be prepared in a given spatial mode, so that emitted light would exhibit spatial coherence. This approach, which relies mostly on the *inhibition* of SE into unwanted modes, requires highly reflective 3D photonic crystals at optical frequencies. Though such truly monomode cavities are not yet available, recent developments in this context are very encouraging [19].

In view of the problems in attaining this ideal situation, several simpler but effective alternatives are being pursued. In the remainder of Section 2 we will identify these alternatives, examine their efficiency and look at their limitations. We start our discussion of collection strategies with one of the simplest, the planar microcavity. In this situation the rate of the emitter is not significantly altered, rather the pathways by which it may lose its energy are simply restricted.

At this stage we need to mention the different ways in which the collection efficiency may be defined. We will be using three parameters; η , β and β_u . The first of these, η , is the fraction of the spontaneous emission collected by the collection optics. For example, this could be the fraction of 4π steradians that can be coupled from an isotropic source to an optical fiber using a simple lens. This is the most obvious parameter associated with collection efficiency and will be the one we refer to most frequently.

The situation is somewhat more complex in cavity QED approaches. Where cavity QED effects are used to ensure emission is predominantly into one mode we need to consider the collection efficiency of that one mode. In this case we need to consider the second and third parameters, β and β_u . β is the fraction of the spontaneous emission that goes into one particular single mode – the desired mode. (This mode may be single even to the extent of being polarized in a particular state.) This fraction β is the important parameter in micro-lasers but less immediately useful here since it does not tell us how well this desired mode is collected by the collection optics. The parameter β_u is used for this purpose; it is the fraction of the spontaneous emission that is both emitted into the desired mode and collected by the collection optics. In general β_u will be less than β . This is due to both photons in the desired mode being wasted, *e.g.*, through scattering by roughness and because the collection optics may not be able to collect all photons emitted by the mode. For the purposes of comparison we can make the rough approximation that $\eta \approx \beta_u$, thus allowing us to compare multi-mode and single mode systems. We have mentioned these facts because some quantum key distribution schemes require photons of a given polarization and these may be produced from cavity QED schemes where only emission

into a truly single mode is used. However, these are subtleties that are not yet the most important factors since present collection efficiencies are so low. As efficiencies increase the question of whether the photons produced by the source all come from the same mode will become more important. To facilitate comparison between the different approaches discussed here we quote figures for the collection efficiency η throughout, discussing the other parameters where appropriate.

2.1 Planar microcavities

The planar microcavity is perhaps the most extensively studied system owing to the very similar nature of the problem of improving the efficiency of light emitting diodes. Several authors have studied this problem in depth and discussed the merits and problems of alternative microcavity schemes [17, 20–24]. Here we will restrict ourselves to a summary of this work, presenting representative results and calculations to inform our discussion.

Placing the emitter in a microcavity leads to the fields produced by the source being reflected back to the emission site; these reflected fields act to drive the emitter. If the reflected (and retarded) field is in phase with the source then emission will be enhanced; conversely, if it is out of phase emission will be inhibited. Another way to view the effect of the microcavity is that the microcavity alters the allowed electromagnetic modes in the vicinity of the source; if the emitter is in resonance with the mode then emission will be enhanced and *vice versa*. If the number of modes can be restricted to just one then we will have gained full control over the emission. This approach cannot fully be accomplished in practice owing to various limitations to be discussed below, notably losses associated with the cavity mirrors.

In its simplest form the microcavity consists of a wavelength thick slab of emissive material sandwiched between two mirrors. There are two choices for the mirrors; metals and distributed Bragg reflectors (DBR). Hybrid structures employing one mirror of each type are also possible and are often convenient from a fabrication standpoint; a substrate can be prepared in the form of a Bragg mirror, the emissive layer can then be deposited, and a metallic top mirror can then be applied. It might be assumed that metals are not a wise choice for mirrors since they exhibit absorption and may thus reduce efficiency; they are also known to support non-radiative surface plasmon (SP) modes, modes that constitute another loss mechanism. However, microcavities based on Bragg reflectors have their problems too, notably because Bragg mirrors do not act as good reflectors for all wavelengths and all angles of emission, some photons thus “leak” away.

As described above, the effect of the mirrors is to alter the allowed modes in the immediate environment of the emitter. The dispersion diagram for a microcavity is shown schematically in Figure 2. Here the frequency and in-plane wavevector of the allowed modes have been sketched. To maximize efficiency, the best strategy is to

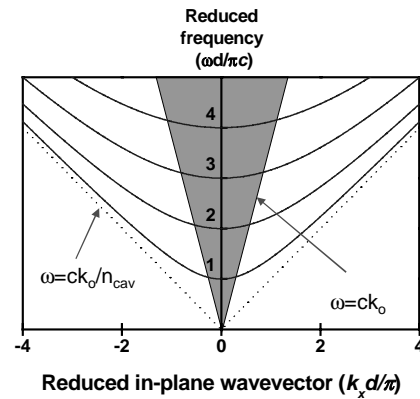


Fig. 2. Schematic dispersion diagram (angular frequency (ω) vs. in-plane wavevector (k_x) of modes of a microcavity having perfectly reflecting mirrors, separated by a distance d . The light line $\omega = ck_0/n_{cav}$ represents the maximum in-plane wavevector a mode photon can have in the cavity material, refractive index n_{cav} . The shaded region represents those wavevectors within the light line for air $\omega = ck_0$ and thus represents the region of the dispersion diagram for which modes may be collected given a collection optics system with $NA = 1$.

ensure that the microcavity supports only the lowest order mode at the emission frequency (*i.e.* the mode with reduced frequency equal to 1 in Fig. 2). By having only one mode into which emission may take place the emission into unused, “wasted” modes is minimised. Further, by making the emission frequency resonant with this microcavity mode the emission emerges from the microcavity primarily in the forward direction, ideal for our purposes.

The particular choice of mirror combination makes surprisingly little difference to the overall efficiency [24]. We choose to examine a hybrid DBR/metal mirror system since this is a well-proven technology in the context of organic light emitting diodes. For this system the calculated efficiency for emission into the full half space above the microcavity ($NA = 1$) is $\eta = 41\%$ and into a cone of angles corresponding to a numerical aperture of $NA = 0.5$ the efficiency is $\eta = 30\%$. For an all-metal cavity these figures are 32% and 17% respectively. These figures are based on emission in the red part of the spectrum and for refractive indices typical of organic systems containing dye molecules. The less than 100% efficiency is due to emission that leaks through the Bragg mirrors, associated with the limited angle range over which they reflect mentioned above, and losses in the metal. The losses associated with the metal are due to both direct excitation of electron-hole pairs etc. and *via* the generation of surface plasmons. Improving the microcavity as it is used here will require the dimensionality to be reduced. This is a topic we will discuss in Sections 2.2 and 2.3. However here we wish first to focus on another problem common to many single photon sources, that of broadband emission.

Our discussion so far has tacitly assumed that the emitter produces photons in a narrow spectral band. This is often not the case and has important implications for the collection efficiency. The schematic microcavity dispersion

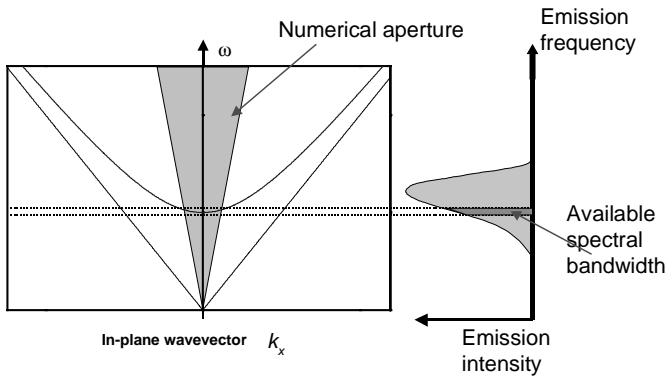


Fig. 3. Only part of the emission spectrum of a broadband emitter embedded in a microcavity may couple to modes that can be collected with finite NA optics.


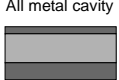
Structure	$\eta(NA=1)$		$\eta(NA=0.5)$		
	Spectrum	Narrow	Broad	Narrow	Broad
 Metal/DBR cavity		41%	34%	30%	10%
 All metal cavity		32%	27%	17%	8%

Fig. 4. The calculated collection efficiency for a spectrally broad ($\Delta\omega/\omega = 20\%$) and a spectrally narrow emitter (*i.e.* a delta function) from within two cavity type structures; a hybrid cavity (upper) and a metallic cavity lower. Material parameters appropriate to the organic emissive system based on Alq₃ were chosen. For this material the peak emission is at 550 nm, the width is ~ 120 nm. The hybrid cavity DBR comprised two $\lambda/4$ layers of each of the high index ($n = 2.26$) and low index ($n = 1.46$) materials. Thicknesses of the layers were chosen to optimize the desired output. The frequency dependent complex dielectric constant for the silver was taken from experimental data [52].

diagram is re-shown in Figure 3, together with a broadband emission spectrum. Whilst the emission may predominantly couple to the lowest order microcavity mode, it will be produced over a wide range of emission angles. As Figure 4 shows, the effect of the broadband emission on the collection efficiency is particularly marked when a collection solid angle of less than $NA = 1$ is used; a substantial fraction of the emitted photons then fall outside the collection cone because they are too far off the resonance frequency. Whilst the spectral filtering of broadband emission in this way is advantageous because it facilitates extra filtering in the detection optics of an optical channel, the reduced efficiency is not so welcome. The planar microcavity with its somewhat limited cavity QED effect is thus not ideal for broadband emission systems. Such systems are perhaps better served by a geometrical approach, notably the solid immersion lens to be discussed in Section 3.1.

It might be thought that the cavity QED approach has little future if solid immersion lenses can be successfully

implemented. However, this is only the case if we restrict ourselves to planar 2-dimensional systems; greater cavity QED effects can be accomplished if we are able to reduce device dimensionality [25]. Below we discuss three alternatives that do just that, microcavities containing wavelength-scale periodic microstructure, individual pillars etched out of planar microcavities, and a more speculative approach using surface plasmons.

2.2 Textured microcavities

There are two main ways in which texturing an otherwise planar microcavity on the scale of the wavelength of light may help. In the first the microstructure simply acts to couple wasted guided modes to radiation [26–28]. This approach, in which a guided mode scatters off the microstructure to emerge as useful radiation has recently been used to improve the efficiency of light emitting diodes [29]. Many variants of this approach have been tried in the context of LEDs however, one has to take care in considering these variants for single photon source applications since many rely on transferring the effective emission point laterally by a macroscopic amount, out of the collection spot of a microscope objective (or similar component) used to direct the photons into the collection optics. Typically this will lead into emission into multiple modes. For this reason truncated pyramid structures are probably not appropriate [30]. For this textured microcavity approach to work efficiently it is preferable for the microcavity to support only one mode. Microcavities based on DBR mirrors can never meet this objective owing to the leaky modes propagating predominantly in directions parallel to the mirror surfaces that they support. On the other hand the lowest order mode supported by microcavities based on metallic mirrors is the surface plasmon mode; in this context one must therefore attempt to use the surface plasmon mode as the channel by which to collect single photons; this is discussed further in Section 2.5. We should perhaps note that design tools to evaluate the limits that may be reached by this approach are not yet readily available.

There is a second aspect to the use of microstructure that may have an important bearing on collection efficiency. If the modulation of the cavity is sufficiently strong then photonic band gaps may result. These are frequency regions in which no modes may propagate in the microcavity. Whilst it may be possible to block unwanted microcavity modes in this way [31] as was discussed at the beginning of Section 2, a more interesting approach would be to use the photonic band edge associated with a photonic band gap [32, 33]. This is a region with a high density of photonic states and has the potential to dynamically channel energy into one well-defined mode. More will be mentioned on this subject in Section 2.5 where we look at a rather intriguing microcavity mode, the surface plasmon. Before looking at surface plasmons we turn our attention to one of the most successful implementations of cavity QED in the solid state, that of pillars.

2.3 Micropillars

Considerably more control over emission can be accomplished than in the planar microcavities discussed in Section 2.1 if some kind of confinement in the plane of the microcavity can be added. In this way significant selective enhancement of spontaneous emission into a given mode can be achieved. As predicted by Purcell in 1946 [34], a radiating dipole placed on resonance with a cavity mode can experience a strong enhancement of its spontaneous emission rate. In the solid-state, the Purcell effect has been observed for InAs quantum dots in micropillars [35–37], micro-discs [38] and VCSEL-like oxide-apertured microcavities [39]. For an ensemble of quantum dots spontaneous emission rate enhancement factors as large as 5 for micropillars and 18 for microdisks have been observed. Even stronger effects are observed on single quantum dots when they are well matched spectrally with the cavity mode, and located close to its spatial antinode [37,38].

It is clear that micropillars and microdisks, in common with microspheres or 1D/2D photonic bandgap microcavities are not perfect “photonic boxes”. These cavities support a continuum of non-resonant modes, besides their set of discrete resonant cavity modes. Since the Purcell effect enhances *selectively* the emission into the resonant cavity mode, it allows one to couple most of the spontaneous emission into that mode. More precisely, the fraction of spontaneous emission (β) coupled into a single desired mode can be written as:

$$\beta = \frac{F/\tau_0 - \gamma/\tau_0}{F/\tau_0} = \frac{F - \gamma}{F} \quad (2)$$

where $1/\tau_0$ is the reference spontaneous emission rate in free space, F is the enhancement factor of the total spontaneous emission rate with respect to its free space value, and γ/τ_0 the spontaneous emission rate into unwanted modes. Experimentally, γ/τ_0 can be extracted from the study of an emitter which is out-of-resonance (either at lower or higher energies than the cavity mode), and which is therefore only coupled to unwanted modes of the microcavity. For micropillars [35] or microdisks [38], the spontaneous emission rate into leaky modes is comparable to the free space value, *i.e.* $\gamma \sim 1$. For a single QD in a micropillar such that $F > 10$, we obtain $\beta > 0.9$ thanks to the Purcell effect, a dominant fraction of the SE is dynamically funneled into the cavity mode.

Unfortunately this “nearly” single-mode coupling is not enough to ensure that a large fraction of the spontaneous emission will be collected and therefore useful. The remaining problem is still one of collection. This is especially clear in a related structure, that of the microdisks, photons in the whispering gallery mode of a disc can escape the cavity in all directions around the plane of the microdisks, so that only a small fraction of the spontaneous emission would be collected by *e.g.* a conventional micro-photoluminescence set-up based on a microscope objective.

Micropillars appear to be better suited for photon collection since their far-field emission is well collimated; for

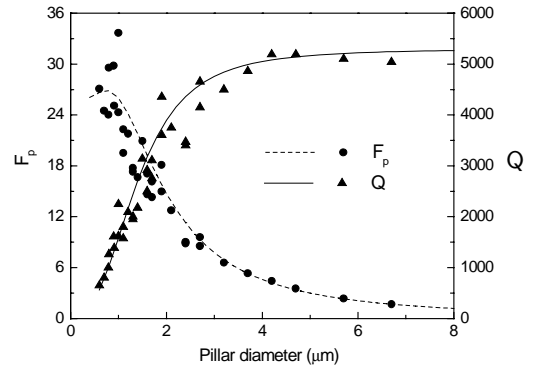


Fig. 5. Q and F_P for a series of micropillars ($Q_0 = 5000$); dots: experiment; lines: theory.

a $1 \mu\text{m}$ micropillar and at a wavelength of $1 \mu\text{m}$, the beam divergence is of the order of 12° , *i.e.* smaller than the acceptance angle of a conventional optical fiber [40]. However efficient photon collection should not be taken for granted and requires careful optimization of the micropillar structure as explained below.

Let us first consider a micropillar built with balanced DBRs. Since the photon has equal probability to escape the cavity from the top or from the bottom, the useful fraction of the spontaneous emission, referred to as β_u in the following, would be equal to $\beta/2$. Though we can easily ensure that photons mostly escape the cavity through the top mirror, this simple example shows that β_u and β need not be identical.

In practice, scattering induced by sidewall roughness is the main subject of concern in this context. As shown in Figure 5, this effect is highlighted by studies of the cavity quality factor Q (measured for the fundamental mode of circular micropillars) as a function of the pillar size. For large pillar diameters, Q is constant and equal to the planar cavity quality factor Q_0 . Below a certain critical diameter, a degradation of Q is observed. This shows that the photon lifetime in the cavity is reduced due to the onset of a new escape path related to scattering by sidewall roughness. The experimental behavior for Q is well described by a simple model that assumes the scattering probability is proportional to the mode intensity at the surface of the pillar, supporting the interpretation given above. These experimental data allow one to estimate the fraction of the photons, initially emitted into the cavity mode, which exit the cavity through the top mirror. Since cavity losses are small, one may write,

$$\frac{1}{Q} = \frac{1}{Q_0} + \frac{1}{Q_{\text{scat}}} \quad (3)$$

which says that the total losses are due to top mirror losses and to losses related to sidewall scattering. Experimentally the first two terms can be measured so that we can easily estimate the useful fraction of the spontaneous emission as,

$$\beta_u = \beta \frac{Q}{Q_0}. \quad (4)$$

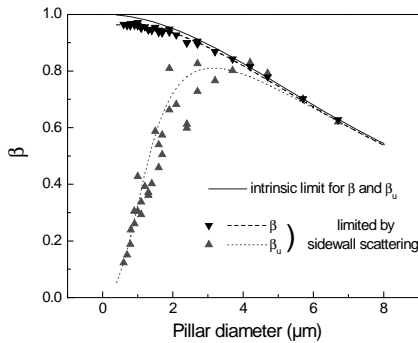


Fig. 6. Estimates of β and β_u for the same series of micropillars as Figure 5 ($Q_0 = 5000$).

When cavity losses due to sidewall scattering are dominant, β_u can be much smaller than β . This has a strong impact on the design of pillar microcavities as illustrated now for state-of-the-art micropillars.

2.4 Design rules of pillar microcavities in view of photon collection

Until now most of the effort on quantum dots in cavities has been concentrated on maximizing of the magnitude of the Purcell effect (thus maximizing β . This lead to a search for micropillars exhibiting high Purcell figures of merit, F_P , given by,

$$F_P = 3Q(\lambda/n)^3/4\pi^2V \quad (5)$$

where V is the effective volume of the resonant mode, n the refractive index at the antinode of the field and λ the wavelength in vacuum.

This procedure is not optimal as far as β_u is concerned for two reasons. Firstly, it tends to favor low V cavities, for which losses due to sidewall scattering are larger. Secondly, high finesse planar cavities are also preferred, since a large Q_0 helps reduce total losses; this again increases the relative role of scattering losses compared to intrinsic (mirror) losses.

We plot as an example in Figure 6 estimates of β_u and β for a state-of-the-art series of micropillars, obtained from the etching of a high finesse planar microcavity ($Q_0 = 5000$). In particular, $1 \mu\text{m}$ diameter micropillars from this series exhibit record Purcell figures of merit, in excess of 30 (Fig. 5). We assume the emitter is a single, quasi-monochromatic QD, located at the antinode of the mode, and spectrally perfectly on resonance. The QD dipole is randomly oriented, so that its emission rate into each of the two polarization-degenerate modes of the pillar microcavity is $F_P/(2\tau_0)$. β and β_u , calculated for the (degenerate) fundamental mode can be written as:

$$\beta = \frac{F_P}{F_P + \gamma}; \quad \beta_u = \frac{Q}{Q_0} \frac{F_P}{F_P + \gamma}. \quad (6)$$

For a micropillar with anisotropic cross-section and non-degenerate fundamental mode, F_P should be replaced by $F_P/2$ in these expressions.

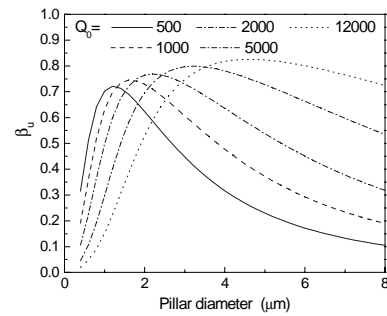


Fig. 7. Pillar diameter dependence of β_u for different values of Q_0 , for a state-of-the art sidewall roughness (the Q vs. diameter values are the best we are aware of, indicating the roughness is the smallest yet achieved by the reactive ion etching process used for these materials).

In Figure 6 dots correspond to estimates based on the experimental measure of Q and Q_0 and on a calculation of V . Solid lines are guides for the eye, calculated using for Q the fitting curve shown in Figure 5. Some important conclusions can be made at this point. Firstly, β does not go to unity for small pillar diameters since F_P displays a maximum around $1 \mu\text{m}$. However, in spite of sidewall scattering, large values of β are obtained as soon as the Purcell factor is much larger than one, and β is not too far from its intrinsic limit. Secondly, sidewall scattering plays a much more important role for β_u . Since intrinsic cavity losses are very weak (large Q_0), additional losses due to sidewall scattering become dominant for diameters below $3 \mu\text{m}$, so that further reducing the pillar diameter is very detrimental. (Our discussion here refers to the specific material system we have chosen, GaAs/AlAs – other materials are likely to differ in the specific dimensions at which pillar sizes are optimal.) Third, an optimum useful fraction of the spontaneous emission of the order of 0.8 can be obtained around $d = 3 \mu\text{m}$ for such state-of-the-art, high Q micropillars.

In practice, the choice of the pillar diameter d may be defined by other constraints; size reduction is for instance frequently used to reduce the number of emitters present in the micropillar. In such a case, it will be necessary to choose Q_0 in such a way that scattering losses remain smaller than intrinsic cavity losses for the diameter of interest. In order to illustrate this point, we plot in Figure 7 an estimate of β_u for different planar cavity finesesses Q_0 . We assume here that the sidewall roughness is constant from process to process and identical to the one observed in our previous experiment.

Quite interestingly, this calculation shows that large values of β_u ($\beta_u > 0.7$) can be obtained for diameters in the $1\text{--}4 \mu\text{m}$ range, provided an appropriate value is chosen for Q_0 . We see also that technological constraints limit the collection efficiency of micropillars. Even for the best Q_0 reported (11700 [41]), and for a state-of-the-art processing, β_u will only reach about 0.83. It is also worth noticing that the maximum value of β_u does not depend much on Q_0 . This behavior enables one to choose the pillar diameter (if necessary) without compromising too much

the collection efficiency β_u , provided an appropriate value is chosen for Q_0 .

Our discussion of micropillars shows what can be done with the impressive nano-fabrication facilities currently available. Given a well-designed structure and the low beam divergence of the mode, we can approximate the collection efficiency as $\eta \sim \beta_u \sim 70\%$. However, the opportunities presented by micropillars depend on the source having a narrow emission spectrum. If we wish to take advantage of the Purcell effect we need a Purcell factor (F_P) of at least 1. From the data shown in Figure 5 this corresponds to a Q of ~ 100 . Thus at an operating wavelength of $1 \mu\text{m}$ ($\sim 1 \text{ eV}$) the source must have a bandwidth of less than 10 nm ($\sim 10 \text{ meV}$). Not all single emitter sources will be amenable to this approach, particularly those with broadband emission spectra, such as defect centers in diamond. With this in mind we now briefly discuss an alternative based on surface plasmons.

2.5 Surface plasmons

One of the factors that should help achieve high collection efficiency is to use structures that support only one photonic mode. As we discussed in Section 2.1, the only way to accomplish this for a microcavity type structure is either to use a defect mode in a 3D photonic crystal, or to use a metal mirror based microcavity that is thin enough so that it only supports the lowest order guided mode, the surface plasmon mode [42–44]. The idea is to couple the emitter to the surface plasmon mode and then couple the surface plasmon mode to radiation.

Surface plasmons are electromagnetic waves that are guided by the interface between a metal and a dielectric and are coupled to the free electrons of the metal. They have electromagnetic fields that peak at the interface and decay exponentially with distance away from the interface. The coupling of the electromagnetic field to the free electrons leads to surface plasmons having increased momentum when compared to an electromagnetic wave in the dielectric; for this reason such modes are in general non-radiative. In the context of single photon sources surface plasmons might thus seem a rather perverse approach, given that they are non-radiative and damped, owing to absorption in the metal on which they propagate. However, the dispersion for surface plasmon modes is in general the highest of any guided mode, thus ensuring that a greater spectral bandwidth can be collected into a given numerical aperture than for any other mode. Further, it has been shown that surface plasmons can be efficiently coupled to radiation by Bragg scattering, with efficiencies $\sim 70\%$, accomplished in just the same way that trapped waveguide modes can be recovered using in plane microstructure [45–47]. The limits to this approach are not yet known though previous research [45] indicates that 80% may be possible through appropriate choices of surface profile. Given this recovery efficiency it is interesting to calculate the power coupled to the surface plasmon mode. This type of calculation can be done by making use of suitable theoretical models based on treating the

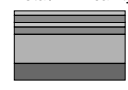

Structure	$\eta(\text{NA}=1)$		$\eta(\text{NA}=0.5)$	
	Narrow	Broad	Narrow	Broad
 Metal/DBR cavity	41%	34%	30%	10%
 SPP system	72%	71%	68%	67%

Fig. 8. Comparison between a planar hybrid microcavity and a textured surface plasmon based system for broad ($\Delta\omega/\omega = 20\%$) and narrow (delta function) band emitters. The hybrid cavity figures are the calculated coupling efficiencies given in Figure 4. The surface plasmon (strictly speaking the surface plasmon polariton – SPP) figures assume a coupling efficiency between the surface mode and radiation of 100% . In practice this is more likely to be $60\text{--}80\%$ for a 2D grating, reducing the figures quoted accordingly [47].

source as a dipole antenna [48]. The results are shown in Figure 8, where for comparison we have also included the results of power emitted by the hybrid DBR/metal planar microcavity. The surface plasmon approach would appear to be advantageous in the case of a broadband emitter and low numerical aperture collection optics; in this case the surface plasmon approach offers an efficiency of approx. 48% (67% coupled by the emitter to the SP mode, $\sim 70\%$ of the mode then coupled to radiation) compared with 10% from the hybrid microcavity, though we note that this has yet to be confirmed by experiment. The refractive index of the emissive layer is important in these calculations, we have assumed an index of ~ 1.7 typical of organic materials – use of higher index materials will lead to lower efficiencies.

Whilst discussing emission mediated by surface plasmons we should note that the mode density associated with surface plasmons may be quite high, especially on microstructured surfaces. Here the microstructure results in a band gap and associated band edge for the surface plasmon mode; at the band edge the mode density is high though it extends over a considerable range of wavevectors. Consequently this approach may yield little net improvement in collection efficiency. However it is still of interest because the band edge may allow one to channel energy dynamically into surface plasmons, thus effectively reducing the bandwidth of the emitter. Again, although this has still to be demonstrated it does offer the prospect of reduced bandwidth and an enhancement of the emission rate; the mode density at a photonic band edge is equivalent to a substantial Purcell factor, perhaps of order 10.

The approaches we have discussed so far have all been based on manipulating the modes into which emission may take place. In the next section we concentrate on an alternative, that of distorting the modes into which the photon is emitted into the mode of the optical collection system, by refraction.

3 Improving the collection efficiency – geometrical approaches

The numerical aperture of the collection optics is limited to $NA = 1$ unless special measures are taken. There are broadly speaking two alternatives, liquid immersion lenses and solid immersion lenses. In both cases the idea is to reduce the index contrast between the emissive material and the immediate surroundings, thereby relaxing the restrictions imposed due to total internal reflection. Subsequently, by use of a highly curved dielectric interface (the lens), the emission is refracted into a suitable mode. Of the two approaches the solid immersion lens is the one of more promise in the present application. The reason is that suitable liquids, such as standard immersion oil, have smaller refractive indices (in the approximate range 1.3–1.75) than solid counterparts (in the range 1.5–3.5). The smaller refractive index translates, *via* Snell's law, to a smaller collection solid angle inside the emissive material. An advantage with liquid immersion lenses is that relatively cheap standard lenses with excellent imaging properties exist.

3.1 Solid immersion lens

A solid immersion lens (SIL) consists simply of a truncated small sphere of high refractive index forming a plano-convex lens of very short focal length. SILs can be bought commercially, but we made the SILs used in our experiments ourselves by polishing a small glass sphere against a flat, and regularly inspecting the result to obtain the proper shape and polished face quality. SILs were first discussed in the context of microscopy by Mansfield and Kino [49], and their potential of coupling light efficiently from a point-like source has previously been identified [50]. SILs discussed in the literature come in one of two designs, the hemisphere and the Weierstrass geometry. The hemisphere is particularly interesting in microscopy applications, since a lens of this design lacks chromatic aberration. This is useful for white light microscopy. In fact, in many high power magnification microscope objectives the front lens element is a hemispherical SIL. In the Weierstrass geometry, the height of the SIL is $(1 + 1/n_2)r$, where n_2 is the refractive index of the SIL and r its radius of curvature, Figure 9. This design leads to a decrease of the angle of refraction γ of the transmitted light, measured from the optical axis. The Weierstrass SIL effectively compresses the emitted light into a small numerical aperture. The price to be paid is poor image forming properties, such as severe chromatic aberration. However, in the context of single emitter collection efficiency the image forming quality of the SIL is of little importance.

We now make a quantitative comparison between the photon collection efficiencies from an emitter located close to the plane surface (that is, much closer than the emission wavelength) of a high refractive index bulk material (such as an overgrown quantum dot) when a SIL is used as a primary collection lens and when the SIL is absent. Let us first consider the case when the SIL is absent (or,

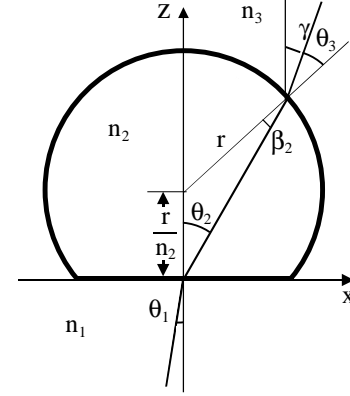


Fig. 9. The geometry of a Weierstrass solid immersion lens.

equivalently, $n_2 = n_3$ in Fig. 9). Snell's law then dictates that

$$n_1 \sin(\theta_1) = n_2 \sin(\theta_2) \quad (7)$$

where n_1 and n_2 are the refractive indices of the bulk material and the collection optics, respectively, θ_1 and θ_2 are the respective propagation angles. In absence of a SIL the numerical aperture (NA) of the collection system is, by definition, $NA = n_2 \sin \theta_0$. If the emitter is modeled as a small dipole oriented parallel to the bulk surface in the x -direction, then the emitted intensity I as a function of the emission angles θ_1 and the azimuthal angle ϕ measured from the x -axis, is

$$I(\theta_1, \varphi) \propto \frac{3}{8\pi} [1 - \sin^2(\theta_1) \cos^2(\varphi)] \quad (8)$$

where the intensity has been normalized so that when integrated over all solid angles it equals unity. Supposing that the photon collection optics has the numerical aperture of NA , the collection efficiency η is given by

$$\begin{aligned} \eta &= \frac{3}{8\pi} \int_0^{\arcsin(NA/n_1)} [1 - \sin^2(\theta_1) \cos^2(\varphi)] \sin(\theta_1) d\theta_1 d\varphi \\ &= \frac{1}{32} \left[15 \left\{ 1 - \sqrt{1 - (NA/n_1)^2} \right\} \right. \\ &\quad \left. + \{1 - \cos[3\arcsin(NA/n_1)]\} \right]. \end{aligned} \quad (9)$$

In (9) it is assumed that no photons are reflected at the interface surface, a somewhat unrealistic situation that requires a very elaborate anti-reflection coating on the surface. However, this result serves as an upper bound for the collection efficiency from a planar bulk dielectric. In Figure 10 we have plotted equation (9) under three different assumed conditions. To make a qualitative estimate of the effect of interface reflection that will prevent the reflected photons from reaching the collection optics we have simply assumed that the reflectivity for all photons, regardless of emission angle and polarization direction, is given by $[(n_1 - n_2)/(n_1 + n_2)]^2$. This assumption is somewhat optimistic and will lead to an overestimate

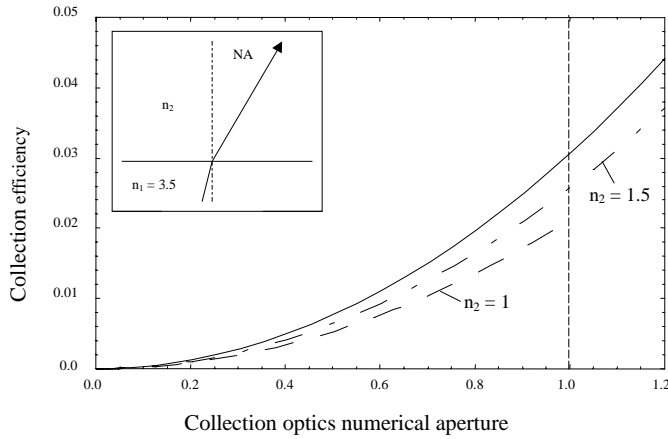


Fig. 10. The calculated collection efficiency through a planar bulk dielectric with refractive index $n_1 = 3.5$. The solid line assumes perfect transmission. The dashed line represents the case where $n_2 = n_3 = 1$ and the interface reflection has been taken into account. (In this case the maximum theoretical collection system NA is unity, indicated by the dotted vertical line.) The dash-dotted curve represents the case when an index matching fluid with $n_2 = n_3 = 1.5$ is used. The corresponding interface reflection is somewhat lower. The boxed inset shows the considered geometry.

of the collection efficiency, as the reflectivity for photons incident on the interface close to the angle of total internal reflection will be close to unity. From the figure it is seen that under relatively realistic assumptions, an ordinary microscope objective with $NA = 0.8$ will collect only slightly over 1% of the total emission. Using a highly refracting $NA = 1.2$ immersion lens with index matching oil ($n_2 = 1.5$), one can only increase the collection efficiency to about 3.5%. Using the best immersion lenses available today, with $NA = 1.6$, it follows from equation (9) that the collection efficiency will still not be higher than 7.8%.

The situation is improved if a hemispherical SIL is centered directly over the emitter. We will assume that the emitter is sufficiently shallowly embedded in the bulk dielectric to be considered as located at the hemisphere center. (In our samples, that are discussed later, the emitter is located only a fraction of a wavelength from the bulk dielectric surface.) In this case, the angle of propagation inside the hemisphere is given by equation (7). However, since every ray exits the hemisphere in a direction normal to its surface, no refraction takes place there, leading to $\theta_3 = \theta_2$. Due to the geometry no total internal reflection can take place for any photon propagating in the SIL. The maximum propagation angle inside the bulk material that will produce a ray lying within the NA of the collection system is,

$$\theta_{1,\text{Max}} = \arcsin\left(\frac{n_2 NA}{n_1 n_3}\right). \quad (10)$$

Replacing the expression NA/n_1 in equation (9) with $(n_2 NA/n_1 n_3)$, we obtain the collection efficiency when a hemispherical SIL is used. In Figure 11 we have plotted

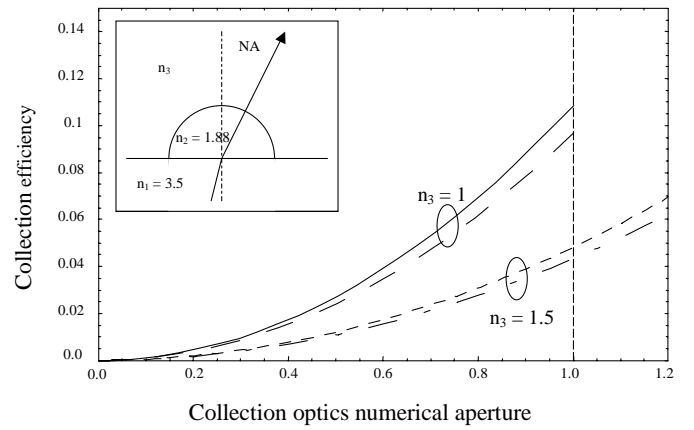


Fig. 11. The calculated collection efficiency from a planar bulk dielectric with refractive index $n_1 = 3.5$ covered by a SIL hemisphere with $n_2 = 1.88$ (the refractive index of LaSFN9 glass). The solid line assumes $n_3 = 1$ and perfect transmission. The long-dashed line represents the case where the interface reflections have been taken into account. The short dashed line represent $n_3 = 1.5$ and perfect transmission. Finally, the dash-dotted curve represents the latter case with interface reflections included.

the results. In the curves including interface reflections, the transmission has been assumed to be,

$$\left[1 - \left(\frac{n_1 - n_2}{n_1 + n_2}\right)^2\right] \left[1 - \left(\frac{n_2 - n_3}{n_2 + n_3}\right)^2\right] \quad (11)$$

irrespective of the propagation angle or the polarization direction. Using an ordinary microscope objective with $NA = 0.8$, and taking interface reflections into account, we see that about 6% of the emission can be collected with the use of a hemispherical SIL. Using a $NA = 1.2$ oil immersion objective will not improve the situation. If we use a hemisphere of the same refractive index as the bulk dielectric, the collection efficiency is further improved. In Figure 12 the predictions for an index $n_2 = 3.5$ hemisphere are shown. It is seen that trivially, a collection system with $NA = 1$ will in principle collect half the emitted photons (all photons emitted in the 2π steradians toward the surface). Taking the reflections into account, and assuming a more realistic collection optics $NA = 0.8$ (in air), one can hope to collect as much as 17% of the emitted photons. This is a very substantial improvement from the bare planar surface case. In this case it does not help to use an oil immersion collection lens unless its numerical aperture exceeds 1.1. Even with a $NA = 1.2$ such an objective will “only” collect between 20 to 25% of the emission.

The collection efficiency as a function of the collection optics numerical aperture can be further improved by going from the hemispherical geometry to the Weierstrass geometry. In this case, the SIL is made slightly higher than a hemisphere, its height along the optical axis is $(1 + 1/n_2)r$. In this case the price to be paid is that the lens has substantial aberration and a severe image distortion. However, in situations where the emission is narrow

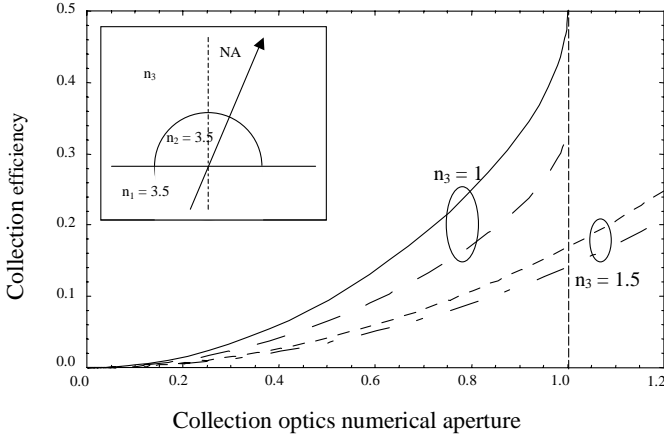


Fig. 12. The calculated collection efficiency from a planar bulk dielectric with refractive index $n_1 = 3.5$ covered by a SIL hemisphere with $n_2 = 3.5$. The solid line assumes $n_3 = 1$ and perfect transmission. The long-dashed line represents the case where the interface reflections have been taken into account. The short-dashed line represent $n_3 = 1.5$ and perfect transmission. Finally, the dash-dotted curve represents the latter case with interface reflections included.

band, so that the chromatic aberration can be ignored, and the emitter is very small, so that image distortion is irrelevant, the Weierstrass geometry offers the highest efficiency (for systems where $n_1 < n_2$). It is readily shown that, for this geometry, the collection angle γ is related to the emission angle θ_1 through,

$$\gamma = \arcsin \left[\frac{n_1}{n_2} \sin \theta_1 \right] + \arcsin \left[\frac{n_1}{n_2^2} \sin \theta_1 \right] - \arcsin \left[\frac{n_1}{n_2 n_3} \sin \theta_1 \right]. \quad (12)$$

For a Weierstrass sphere surrounded by air, this expression simplifies to,

$$\gamma = \arcsin \left[\frac{n_1}{n_2^2} \sin \theta_1 \right]. \quad (13)$$

If we recall that only photons with $\theta_1 < \sin^{-1}(n_2/n_1)$ will be transmitted through the bulk dielectric-to-SIL interface, we see that all the transmitted photons will be refracted by the SIL within a numerical aperture $NA < 1/n_2$ in the surrounding air. Replacing the expression NA/n_1 in equation (9) with equation (13), and integrating only to $NA = 1/n_2$, we can once more estimate the collection efficiency. In Figure 13 the result is shown. We see that for an optimally AR coated Weierstrass sphere with $n_2 = 1.88$ the upper bound for collection efficiency is 11% (the same as for the SIL hemisphere), but this value is achieved for a collection system NA of about 0.53, instead of unity in the hemisphere case. This is convenient, because in order to filter out an individual exciton line from a semiconductor quantum dot, the dot needs to be cooled to cryogenic temperature [15,51]. This has the

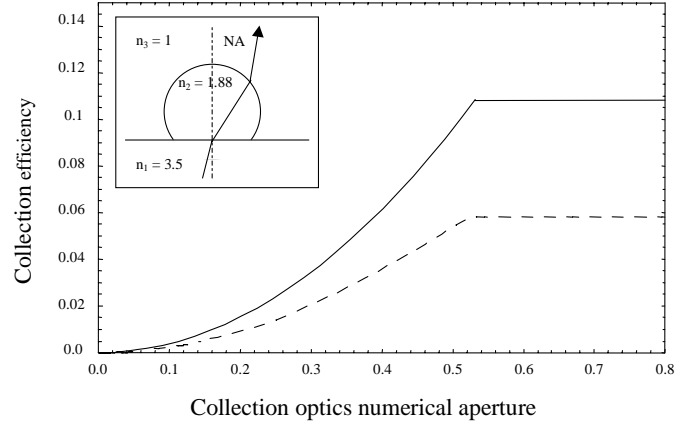


Fig. 13. The calculated collection efficiency from a planar bulk dielectric with refractive index $n_1 = 3.5$ covered by a Weierstrass SIL with $n_2 = 1.88$ into air ($n_3 = 1$) assuming perfect transmission at all interfaces. The short-dashed line is the Monte-Carlo simulation with all interface reflections included.

undesired side effect that the collection optics typically will have to be located a few mm away from the sample, and consequently the collection objective NA will more typically be around 0.5 than unity. In practice, placing a Weierstrass sphere on top of the quantum dot, inside the cryostat, will greatly increase the collection efficiency. A drawback of the Weierstrass geometry is that the laser excitation cannot easily be delivered at an angle outside the collection optics numerical aperture. Instead, it must be incident parallel to the optical axis, that effectively means through the objective. This requires careful filtering of the collected light. A hemispherical SIL is simpler to use from the excitation point of view, since collimated light propagating along any radial of the hemisphere will be focused at the hemisphere center. Hence, the sample can be excited by light propagating outside of the collection objective numerical aperture.

To make a realistic estimate of the collection efficiency from a Weierstrass sphere, including the interface reflectivity, we have used a Monte-Carlo method. The emission angle θ_1 is stochastically generated in the interval $[0, \pi/2]$ with the normalized probability distribution $P(\theta_1 = \theta) = \sin \theta$. This distribution takes care of the available solid angle as a function of θ_1 . The simulated photons are subsequently ray-traced through the hemisphere, using the Fresnel reflection formulae to take into account the interface reflections. Note that the geometry of the Weierstrass sphere is such that no photon directly transmitted from the bulk dielectric into the sphere undergoes total internal reflection. However, some photons will be reflected at the sphere interface, in particular those photons with θ_2 close to $\pi/2$. However, in the case we consider the reflected photons will only contribute to the emitted intensity at angles γ of about $\pi/2$ and above. To see why this is the case, let us consider the fate of a photon emitted so that it strikes the Weierstrass SIL at the equatorial plane, lying

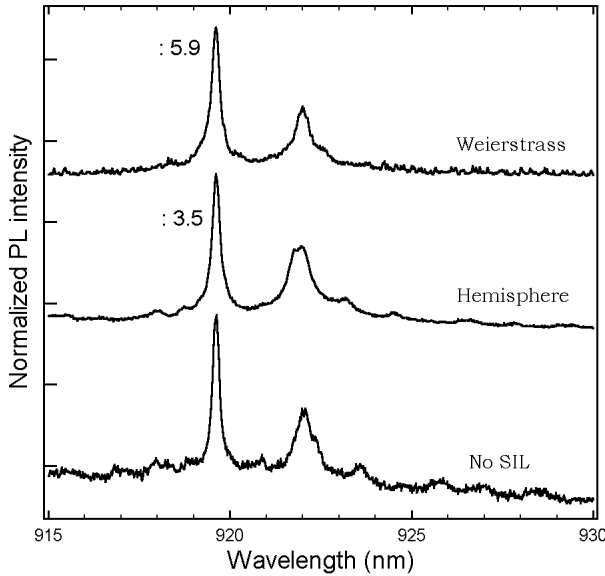


Fig. 14. The measured photoluminescence spectra for a InAs quantum dot embedded in GaAs using a $NA = 0.4$ microscope objective. From top to bottom the spectra are measured using no SIL, a hemispherical SIL, and a Weierstrass SIL, respectively. The SILs were made from LaSFN9 glass ($n_2 = 1.88$). The spectra are normalized relative to the no SIL case, the normalization factors are indicated for the hemisphere and Weierstrass SILs.

a distance r/n_2 above the bulk dielectric-to-SIL interface. We can readily compute that $\theta_2 = \arctan(n_2) \sim 1.08$ rad $\sim 69^\circ$, and that $\beta_2 = \arcsin[\sin \theta_2/n_2] \sim 0.49$ rad $\sim 31^\circ$. After being reflected at the equator, a photon initially propagating towards the right, will propagate towards the left, and using the reflection law and Snell's law, one finds that this photon will exit the SIL at an angle $\theta_3 = \beta_2 - \theta_2 - \pi/2 \sim -1.67$ rad $\sim -97^\circ$, where θ_3 is positive angle from the z -axis in the clockwise direction. That is, this photon that has been reflected once, will propagate toward the bulk dielectric surface at grazing incidence when exiting the SIL. However, the intensity from these photons is very small, their total contribution of the photons transmitted through the interface and internally reflected by the SIL is on the order of a few percent. Hence, all photons reflected inside the SIL have been considered lost, making our collection efficiency estimation slightly conservative. In Figure 13 we see that the Monte-Carlo simulation predicts that about 6% of the total emission can be collected with a $NA = 0.53$ objective if $n_2 = 1.88$.

To demonstrate the viability of SILs, we show in Figure 14 photoluminescence (PL) spectra from a single InAs quantum dot embedded in GaAs ($n_1 = 3.5$). A $NA = 0.4$ aperture lens was used, and the emission was spectrally dispersed by a monochromator. The ensuing spectra were acquired with a cooled CCD camera. The two SILs employed had a diameter $d = 3$ mm, and were made from LaSFN9 glass with $n_2 = 1.88$. The quantum dot sample was held at 9 K inside a cryostat designed for microscopy.

The SIL was placed directly on top of, and in direct contact with, the sample, inside the cryostat. The alignment of the SIL was made “by hand”, because it is not very critical (it suffices to place the SIL optical axis within a fraction of a mm of the quantum dot) since, to some extent, a misalignment between the quantum dot and the SIL optical axis can be compensated by translating the collection microscope objective relative to the sample with the attached SIL. We see that the ratios between the count rates for using no SIL and using a SIL are about 1:3.5 and 1:5.9 for the hemisphere, and the Weierstrass geometry, respectively. The theory above predicts the ratios 1:3.4 and 1:12, respectively. The ratios are more or less independent of the collection system numerical aperture as long as it is smaller than about 0.5. The important point to note is that SILs offer a substantial improvement in collection efficiency.

Similar results will hold for a Weierstrass SIL with the same refractive index as the assumed bulk dielectric ($n_2 = 3.5$). In this case, due to the high refractive power of the SIL, all photons emitted into the 2π steradians towards the SIL will be refracted to propagate within a NA of 0.28! Our simulations predict that as much as 31% of the total emission will be transmitted through such an uncoated SIL.

Finally, it is, of course, possible to combine a SIL with some of the methods discussed in other sections. Even the simplest improvement, namely layering the bulk dielectric to form a single appropriately designed back Bragg mirror may more than double the collection efficiency. (Without a back mirror many photons are reflected at the sample-to-SIL interface and disappear forever. With a back mirror, they get a second chance to be transmitted into the SIL. However a Bragg mirror reflects only over a limited angle, whereas a metal reflector has little angular dependence. The latter is preferable.) Designing the quantum dot to be located at the anti-node of the interference “fringe” between the emission propagating in the $\pm z$ -direction, the emission in the normal direction would be resonantly enhanced by a factor of four, while the emission in directions close to the dielectric interface would be suppressed. Such a design is currently being pursued.

4 Discussion, merits of different approaches and prospects

We have looked at a variety of approaches for collecting light produced by solid-state single photon sources. We began by identifying why this issue merits consideration: current collection efficiencies are low enough to degrade the potential performance of quantum key distribution based on single photons; improved collection efficiencies are therefore required. The schemes we have discussed to remedy this situation were broadly categorized into two types. Firstly there were schemes based on cavity quantum electrodynamics in which we try to alter the emission so as to enhance one particular mode into which the source may emit and inhibit other unwanted modes. Secondly,

we considered schemes where we simply try to collect as much of the emerging radiation as possible without trying to alter the way in which the source emits.

The simplest cavity QED approach is to use a planar microcavity, discussed in Section 2.1. Such a technique offers a potential efficiency of approximately $\eta = 40\%$ for a narrow band emitter and lower than this if the emission covers an appreciable bandwidth. Texturing the microcavities (Sect. 2.2) offers the possibility of increasing the extraction efficiency, though by how much has still to be determined. To succeed in using texturing will probably require the use of a cavity that supports only one mode and we discussed the use of the surface plasmon mode for this in Section 2.5. For broader emission the surface plasmon mediated emission discussed in Section 2.5 looks appealing, offering a potential $\eta \sim 50\%$. However, though attractive from these calculations this approach is the most speculative and is the least tested. Micropillars were examined in Section 2.3. They appear to offer the best collection efficiency; $\eta \geq 70\%$ looks to be possible. They also prepare photons in a single mode which as we noted in Section 2 may be important in implementing QKD schemes such as polarization encoding. Set against this is the complexity of the fabrication process needed to make micropillars hosting a single emitter, resonant with the cavity mode.

Finally we looked at a geometric scheme based on the solid immersion lens in Section 3.1. We have indicated that the best available efficiency here is $\eta \sim 30\%$, and is relatively simple to implement. Using a back mirror, efficiencies exceeding 50% should be possible.

From the foregoing it would appear that micropillars are the most efficient way to collect single photons. However, we need to remember that collection efficiency is not the only issue in building a successful solid-state single photon source. Of particular importance is the material system that is chosen. For broadband emitters based on low index (typical of organic materials) the planar textured microcavities and the surface plasmon approach are perhaps the best. For higher index materials, notably inorganic semiconductors, micropillars and SILs may be best. The choice of emissive material in turn depends on other criteria such as stability, repetition rate, operating wavelength, emission bandwidth, operating temperature, cost etc. These will all have an influence on the choice to be made. The different approaches we have explored have their own relative merits and problems. Our intention has been to highlight the issues, to identify the potential of the different approaches and thus provide a resource or future research and development.

The authors are members of the European IST/FET program ("Quantum Information Processing and Telecommunication" project 1999-10243 S4P) and are grateful to the EU for part funding this work. WLB, PTW and JAEW acknowledge support from the UK Engineering and Physical Sciences Research Council. JMG would like to thank B. Gayral, E. Moreau and L. Manin-Ferlazzo. The authors are also grateful for discussions with Jean-Philippe Poizat. Finally the authors would like to

express their appreciation for the support and guidance given by Izo Abram.

References

1. S. Nie, R. Zare, *Ann. Rev. Biophys. Biomol. Struct.* **26**, 567 (1997).
2. M. Bourennane, F. Gibson, A. Karlsson, A. Hening, P. Jonsson, T. Tsegaye, D. Ljunggen, E. Sundberg, *Opt. Expr.* **4** (1999).
3. H.J. Kimble, M. Dagenais, M.L., *Phys. Rev. Lett.* **39**, 691 (1977).
4. A. Imamoglu, Y. Yamamoto, *Phys. Rev. Lett.* **72**, 210 (1994).
5. J. Kim, O. Benson, H. Kan, Y. Yamamoto, *Nature* **397**, 500 (1999).
6. O. Benson, C. Santori, M. Pelton, Y. Yamamoto, *Phys. Rev. Lett.* **84**, 2513 (1999).
7. J.-M. Gérard, B. Gayral, *J. Lightwave Techn.* **17**, 2089 (1999).
8. P. Michler, A. Kiraz, C. Becher, W.V. Schoenfeld, P.M. Petroff, Z. Lidong, E. Hu, A. Imamoglu, *Science* **290**, 2282 (2000).
9. N. Lutkenhaus, *Phys. Rev. A* **61**, 052304 (2000).
10. C. Brunel, L. Brahim, P. Tamarat, M. Orrit, *Phys. Rev. Lett.* **83**, 2722 (1999).
11. L. Fleury, J.M. Segura, G. Zumofen, B. Hecht, U.P. Wild, *Phys. Rev. Lett.* **84**, 1148 (2000).
12. C. Kurtseifer, S. Mayer, P. Zarda, H. Weinfurter, *Phys. Rev. Lett.* **85**, 290 (2000).
13. R. Brouri, A. Beveratos, J.P. Poizat, P. Grangier, *Opt. Lett.* **25**, 1294 (2000).
14. C. Santori, M. Pelton, G.S. Solomon, Y. Dale, Y. Yamamoto, *Phys. Rev. Lett.* **86**, 1502 (2001).
15. V. Zwiller, H. Blom, N. Panev, P. Jonsson, S. Jeppesen, T. Tsegaye, E. Goobar, M.-E. Pistol, L. Samuelson, G. Björk, *Appl. Phys. Lett.* **78**, 2476 (2001).
16. P. Michler, A. Imamoglu, M.D. Mason, P.J. Carson, G.F. Strouse, S.K. Buratto, *Nature* **406**, 968 (2000).
17. H. Benisty, H. De Neve, C. Weisbuch, *IEEE. J. Quant. Electron.* **34**, 1632 (1998).
18. E. Yablonovitch, *Phys. Rev. Lett.* **58**, 2059 (1987).
19. S. Noda, K. Tomoda, N. Yamamoto, A. Chutinan, *Science* **289**, 604 (2000).
20. C. Lin, D. Deppe, C. Lei, *IEEE. J. Quant. Electron.* **30**, 2304 (1994).
21. C. Weisbuch, H. Benisty, R. Houdré, *J. Luminesc.* **85**, 271 (2000).
22. V. Bulovic, V.B. Khalfin, G. Gu, P.E. Burrows, D.Z. Garbuzov, S.R. Forrest, *Phys. Rev. B* **58**, 3730 (1998).
23. A. Dodabalapur, L.J. Rothberg, R.H. Jordan, T.M. Miller, R.E. Slusher, J.M. Phillips, *J. Appl. Phys.* **80**, 6954 (1996).
24. J.A.E. Wasey, W.L. Barnes, *J. Mod. Opt.* **47**, 725 (2000).
25. I. Abram, G. Bourdon, *Phys. Rev. A* **54**, 3476 (1996).
26. H. Rigneault, F. Lemarchand, A. Sentenac, *J. Opt. Soc. Am. A* **17**, 1048 (2000).
27. H. Rigneault, F. Lemarchand, A. Sentenac, H. Giovannini, *Opt. Lett.* **24**, 148 (1999).
28. B.J. Matterson, J.M. Lupton, A. Safanov, M.G. Salt, W.L. Barnes, I.D.W. Samuel, *Adv. Mat.* **13**, 123 (2001).
29. J.M. Lupton, B.J. Matterson, I.D.W. Samuel, M.J. Jory, W.L. Barnes, *Appl. Phys. Lett.* **77**, 3340 (2000).

30. G. Gu, D.Z. Garbuzov, P.E. Burrows, S. Venkatesh, S.R. Forrest, M.E. Thompson, *Opt. Lett.* **22**, 396 (1997).
31. S.C. Kitson, W.L. Barnes, J.R. Sambles, *J. Appl. Phys.* **84**, 2399 (1998).
32. M.G. Salt, W.C. Tan, W.L. Barnes, *Appl. Phys. Lett.* **77**, 193 (2000).
33. J.P. Dowling, M. Scalora, M.J. Bloemer, C.M. Bowden, *J. Appl. Phys.* **75**, 1896 (1994).
34. E.M. Purcell, *Phys. Rev.* **69**, 681 (1946).
35. J.-M. Gérard, B. Sermage, B. Gayral, B. Legrand, E. Costard, V. Thierry-Mieg, *Phys. Rev. Lett.* **81**, 1110 (1998).
36. J.-M. Gérard, B. Gayral, L. Manin, *IQEC*, Nice, France, 2000.
37. G.S. Solomon, M. Pelton, Y. Yamamoto, *Phys. Rev. Lett.* **81**, 3903 (2001).
38. B. Gayral, J.-M. Gérard, B. Sermage, A. Lemaître, C. Dupuis, *Appl. Phys. Lett.* **78**, 2828 (2001).
39. L.A. Graham, D.L. Huffaker, D.G. Deppe, *Appl. Phys. Lett.* **74**, 2408 (1999).
40. H. Rigneault, J. Broudic, B. Gayral, J.-M. Gérard, *Opt. Lett.* (in press, 2001).
41. T. Rivera, J.P. Debray, J.-M. Gérard, B. Legrand, L. Manin-Ferlazzo, J.L. Oudar, *Appl. Phys. Lett.* **74**, 911 (1999).
42. W.L. Barnes, P.T. Worthing, *Opt. Commun.* **162**, 16 (1999).
43. W.L. Barnes, *IEEE J. Light. Tech.* **17**, 2170 (1999).
44. J. Vuckovic, M. Loncar, A. Scherer, *IEEE J. Quant. Electron.* **36**, 1131 (2000).
45. J. Moreland, A. Adams, P.K. Hansma, *Phys. Rev. B* **25**, 2297 (1982).
46. P.T. Worthing, W.L. Barnes, *J. Mod. Opt.* (in press, 2001).
47. P.T. Worthing, W.L. Barnes, *Appl. Phys. Lett.* (in press, 2001).
48. W.L. Barnes, *J. Mod. Opt.* **45**, 661 (1998).
49. S.M. Mansfield, G.S. Kino, *Appl. Phys. Lett.* **57**, 2615 (1990).
50. K. Koyama, M. Yoshita, M. Baba, T. Suemoto, H. Akiyama, *Appl. Phys. Lett.* **75**, 1667 (1999).
51. J.-Y. Marzin, J.-M. Gérard, A. Izrael, D. Barrier, G. Bastard, *Phys. Rev. Lett.* **73**, 716 (1994).
52. R.M. Amos, W.L. Barnes, *Phys. Rev. B* **55**, 7249 (1997).